Simulation-based design of mixed-mode specimens for fracture mechanics tests on fiber-metal laminates

J Keck[1], T Mahrholz[2], L Beyland[3], C Hühne[1]

[1]Composite Design, German Aerospace Center - Institute of Lightweight Systems, Brunswick, Germany
[2]Multifunctional Materials, German Aerospace Center - Institute of Lightweight Systems, Brunswick, Germany
[3]Innovation, German Aerospace Center - Institute of Lightweight Systems, Brunswick, Germany

E-mail: jan.keck@dlr.de, thorsten.mahrholz@dlr.de, lutz.beyland@dlr.de, christian.huehne@dlr.de

Abstract. Fiber-metal laminates (FMLs), particularly those composed of glass-fiber-reinforced polymers (GFRP) and steel, are a promising material combination for applications in wind energy, especially in blade root connections. These laminates exhibit complex fracture behavior that requires advanced modeling techniques to accurately predict crack propagation. This study focuses on the simulation of fracture mechanics tests to identify suitable specimen configurations for experimental validation. The investigated crack interface lies at the GFRP-steel interface. Fibers hereby are oriented exclusively in the 0° direction. Different mode-dependent test configurations were considered to determine the critical strain energy release rates (cERR) under varying mode ratios: Double Cantilever Beam (DCB) for mode I, End-Notched Flexure (ENF) for mode II and Single-Leg Bending (SLB), Cracked-Lap Shear (CLS) as well as mixed-mode bending (MMB) for mixed-mode conditions.

The objective is to find specimen configurations allowing to determine critical fracture parameters, including mode I and mode II cERR (G_{Ic}, G_{IIc}), as well as the mixed-mode interaction parameter for the BK criterion (η_{BK}) used to predict crack growth in crack propagation analysis. By simulating multiple mode ratios, a broader range of cERR is assessed to improve the accuracy of crack growth predictions.

A key focus of this work are the mixed-mode specimens providing alternatives to the MMB setup as described in ASTM D 6671. Different layup configurations were analyzed for these specimens by varying the GFRP beam thickness. The resulting specimen designs and accomplished mixed-mode ratios are compared to determine configurations that provide reliable fracture parameter identification.

1 Introduction

One inherent weakness of fiber reinforced plastic materials is their low bearing strength (bolt bearing like in classic T-bolt connection). This usually leads to the necessity of increased laminate thicknesses in the vicinity of bore holes to increase load carrying capacity. This is also the case in wind turbine blades. With increasing length of the blades, higher loads have to be carried by the root connections. To be able to support the higher loads of longer blades one could either increase the bolt circle diameter, and therefore increase the blade root diameter, to achieve higher moments of inertia. However, this solution is not feasible since the height of highway bridges prevents further increases in blade root diameter, when turbine blades are meant to be transported by truck. Therefore the only alternative to still be able to transmit higher loads at the bolted connection of the blade root, is to increase the bearing strength of the laminate.

A promising way to do so are fiber-metal laminates (FMLs). In previous studies by the german aerospace center (DLR) it has been proven, that the bearing strength of glass-fiber-reinforced polymers (GFRP) can be increased by up to 100% when substituting individual glass layers by steel sheets of equal thickness [1]. Since FMLs are only meant to be used in the laminate surrounding the bolt holes, it is necessary to find feasible designs for the transition zone from FML to monolithic GFRP.

Petersen [2] studied the design of such transition zones in FMLs consisting of carbon-fiber-reinforced polymers (CFRP) and steel. He featured the ply substitution technique where individual fibrous plies are substituted by steel layers, instead of introducing additional steel layers into the laminate. The advantage of this technique is that the thickness of the laminate is held constant across the transition zone. In his work, Petersen points out, that delaminations are to be expected as the dominating modes of failure at the transition zones of FMLs. These delaminations are influenced by the design of the monolithic base laminate (fiber orientations as well as number of 0° plies). Further he points out, that applications dominated by bending loads are more prone to delaminations than those experiencing mostly tensile loading. [2]

To design such transition zones and be able to simulate the aforementioned delaminations, interfacial properties in the form of critical strain energy release rates (cERR) are needed. Three different forms of crack opening are usually distinguished: mode I, mode II and mode III. The corresponding cERR can be determined by a variety of fracture mechanics tests. These are for example the Double Cantilever Beam (DCB) and End-Notched Flexure (ENF) tests for cERR in mode I (G_{Ic}) and mode II (G_{IIc}) respectively. DCB and ENF testing are described in ASTM D 5528 [3] and ASTM D 7905 [4].

Since interlaminar crack tips usually feature mixed-mode instead of isolated mode I or mode II loading conditions, knowledge about the relation of cERR and mode ratio is critical. For this reason a variety of mixed-mode tests were developed in the past. The most flexible of which is the mixed-mode bending (MMB) described in ASTM D 6671 [5]. It allows for continuous variation of the mode-mix thanks to the use of a complex test apparatus. However, the downside of this test is, that it can be quite time consuming. So over the years alternative specimens like the Single-Leg Bending (SLB) and Cracked-Lap Shear (CLS) have been developed. While being less flexible in producing different mode mixes, they offer much simpler 3-point-bending or tensile testing procedures. The mode mix is typically influenced by the thickness of the specimen beams. To produce a wide range of mode mixes great differences in beam thickness can be necessary. The vastly asymmetrical laminates resulting from this can be undesirable however, especially in FMLs. Depending on the method of production this can lead to significant warping due to the difference in the coefficient of thermal expansion (CTE) of GFRP and steel.

This paper therefore aims to find alternative specimen designs to the MMB that are still able to span a wide range of mode ratios without the need of vastly asymmetric laminates.

2 Fracture mechanics testing

To be able to simulate crack growth in composite materials, fracture criterions are being used to decide if a crack is propagating. Since the fracture toughness G_c depends on the mode mix present at the crack tip, cERR values for mode I (G_{Ic}), mode II (G_{IIc}) as well as interaction parameters are needed. This will be discussed in more detail in section 3.

A variety of mechanical tests is used to determine these material properties. Tests to produce mode I or mode II and those meant to produce mixed-mode conditions can be distinguished. Examples for mode I and mode II tests are the DCB and ENF. Since these are well known and standardized ([3], [4]) they will be described here only very briefly. Some tests producing mixed-mode conditions are for example the MMB, SLB or the CLS test. These will be discussed in more detail in the following. Common among all these types of fracture mechanics tests is, that they feature a precrack which is extended through the laminate by different kinds of loading.

2.1 Mode I and II tests

The aim of the DCB-test is to produce a mode I crack opening [3]. To do so, hinges are typically fitted to the precracked ends of the specimen. By pulling apart the hinges in a tensile loading machine, the crack is opened normal to the fracture plane. These conditions usually lead to stable crack extension.

In the ENF-test, the crack is being propagated tangentially to the fracture plane, leading to a mode II crack opening [4]. This is achieved by performing a 3-point-bending test on the specimen, leading to a shear loading of the crack tip. This typically leads to unstable crack growth in the specimen.

Both DCB and ENF tests are typically used for composite materials. To ensure pure mode I or mode II conditions at the crack tip, specimens with symmetrical layups should be used, according to the ASTM standards. Otherwise differences in bending stiffness of the upper and lower specimen beam might lead to undesired mixed-mode conditions. This has to be considered when performing DCB and ENF tests on bi-material interfaces as is the case with FML specimens.

2.2 *Mixed-mode tests*

A good overview on the mixed-mode tests available today, is given by [6]. Some of the tests mentioned in [6] will be discussed in the following.

2.2.1 *MMB test*

The MMB test is defined in ASTM D 6671 [5]. Out of all the mixed-mode tests presented here, it offers the greatest flexibility in producing mode ratios. According to the standard, the MMB test is suitable only for determination of interlaminar fracture toughness values of unidirectional composite materials. Specimens are meant to be manufactured from symmetric laminates featuring a crack plane in the center of the specimen.

To achieve the mixed-mode loading conditions on the specimen, a complex apparatus is needed (see figure 1). This is assembled from multiple components, namely the base, lever, yoke, saddle and others. Prior to testing the composite specimens, the compliance of the apparatus has to be measured using a special calibration specimen. This is necessary since the fracture toughness values are being calculated directly from the load-displacement history obtained at the crosshead of the testing machine.

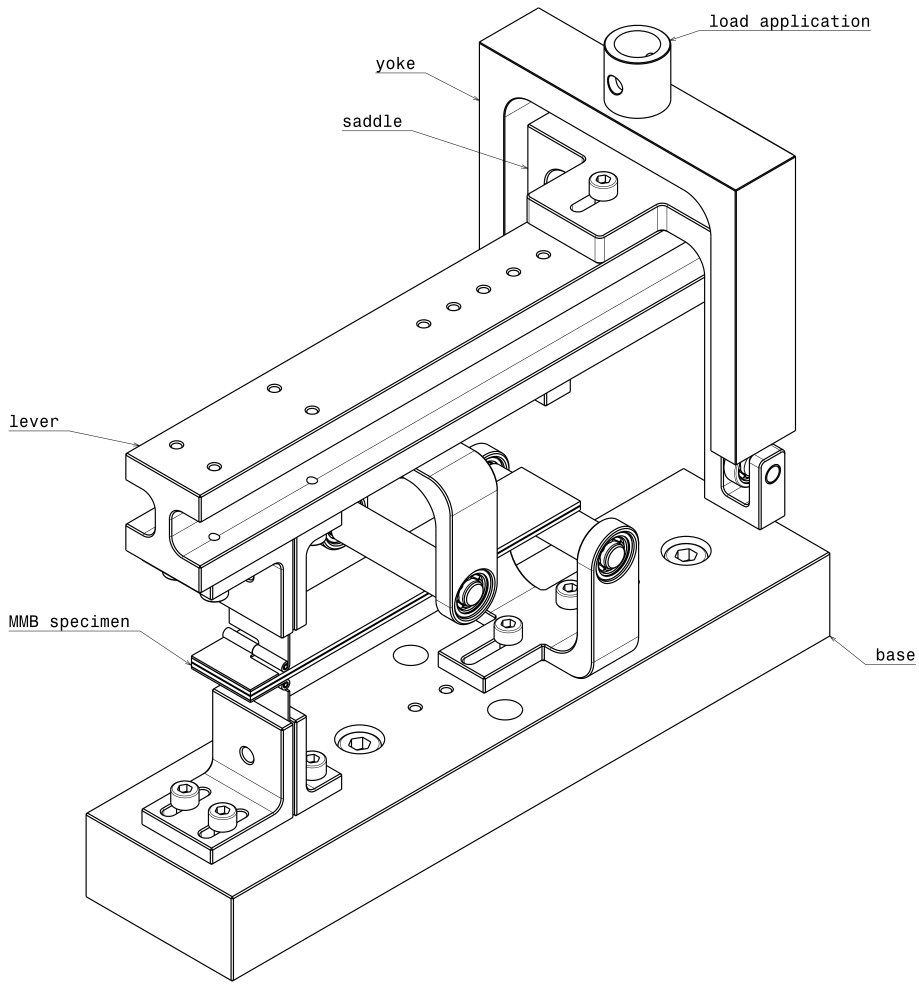

Figure 1: MMB apparatus as suggested by ASTM D 6671.

The mode mixture can be set by manipulating the MMB apparatus. By changing the length c, which marks the distance between the loading point of the lever and the central roller pushing down on the specimen, the G_{II}/G ratio is varied. The MMB apparatus set to two different lever lengths can be seen in figure 2. Equations (1) to (5) relate c to the resulting mode ratios:

$$c = \frac{12\beta^2 + 3\alpha + 8\beta\sqrt{3\alpha}}{36\beta^2 - 3\alpha} \tag{1}$$

$$\alpha = \frac{1 - \frac{G_{II}}{G}}{\frac{G_{II}}{G}} \tag{2}$$

$$\beta = \frac{a + \chi h}{a + 0.42\chi h} \tag{3}$$

$$\chi = \sqrt{\frac{E_x}{11G_{xz}}\left\{3 - 2\left(\frac{\Gamma}{1+\Gamma}\right)^2\right\}} \tag{4}$$

$$\Gamma = 1.18\frac{\sqrt{E_x E_y}}{G_{xz}} \tag{5}$$

where:

h = half thickness of test specimen
χ = crack length correction parameter
Γ = transverse modulus correction parameter

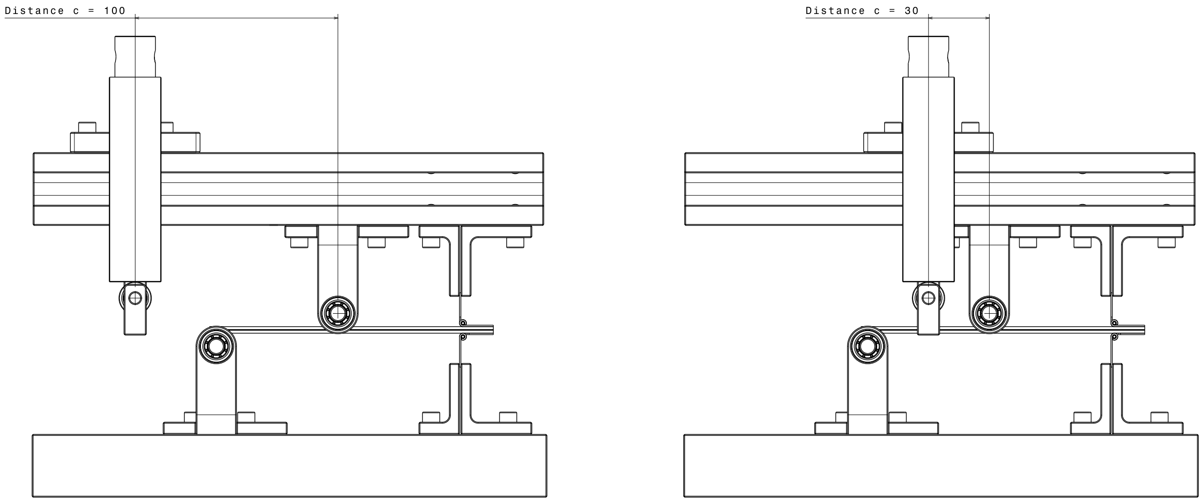

(a) Lever length c = 100 mm

(b) Lever length c = 30 mm

Figure 2: The MMB apparatus set to two different lever lengths.

Load vs. displacement data is recorded during the test and then used to calculate the strain energy release rates and mode mixture G_{II}/G. Total strain energy release rates are calculated as the sum from the mode I and mode II components:

$$G = G_I + G_{II} \tag{6}$$

$$G_I = \frac{12P^2(3c-L)^2}{16b^2h^3L^2E_{xf}}(a+\chi h)^2 \tag{7}$$

$$G_{II} = \frac{9P^2(c+L)^2}{16b^2h^3L^2E_{xf}}(a+0.42\chi h)^2 \tag{8}$$

where:

$$\begin{aligned} a &= \text{delamination length} \\ P &= \text{applied load} \\ L &= \text{half span of MMB apparatus} \\ E_{xf} &= \text{flexural modulus of specimen.} \end{aligned}$$

2.2.2 DCB-UBM

Another fracture test offering a great flexibility in mode ratios is the Double Cantilever Beam with uneven bending moments (DCB-UBM). It was proposed by Søerensen et al. [7] and is a modification of the "classic" DCB testing procedure. Instead of applying normal forces and thereby inducing a bending moment into the specimen beams to open the crack, the DCB-UBM specimen is loaded by applying bending moments directly at the ends of the beams (see figure 3).

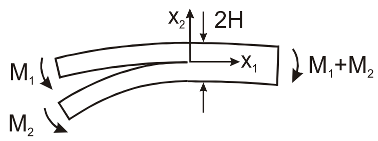

Figure 3: Loading of the DCB-UBM as proposed by [7].

By varying the bending moments M_1 and M_2, different mode ratios can be produced. In fact, this specimen is capable of producing the entire range of mode ratios ranging from pure mode I to pure mode II crack opening [7]. The resulting mode ratio ψ is calculated from the applied moments as follows:

$$\psi = \tan^{-1}\left(\frac{\sqrt{3}}{2}\frac{M_1+M_2}{M_2-M_1}\right). \tag{9}$$

Equation 9 is only valid for homogeneous specimens however. For the case of a bi-material crack interface, as is the case with FMLs, determination of ψ becomes more complicated, as a bi-material specific parameter ϵ is needed:

$$\psi = \tan^{-1}\left(\frac{Im(KH^{i\epsilon})}{Re(KH^{i\epsilon})}\right) \tag{10}$$

with:

$$\begin{aligned} K &= K_1 + iK_2 \\ i &= \sqrt{-1}. \end{aligned}$$

ϵ hereby is defined as [8]:

$$\epsilon = \frac{1}{2\pi} \ln \left[\frac{\kappa_1 \mu_2 + \mu_1}{\kappa_2 \mu_1 + \mu_2} \right] \tag{11}$$

Here, $Im(KH^{i\epsilon})$ and $Re(KH^{i\epsilon})$ are the imaginary and real part of $KH^{i\epsilon}$, with K being the stress intensity factor and H the half specimen thickness.

In [7] the authors used the DCB-UBM to perform fracture tests on GFRP adherends bonded by a 3 mm thick adhesive layer. They employed a test fixture with transverse beams attached to the specimen beams for load introduction. The transverse beams were loaded with identical magnitude, however by changing the distance between the loading points (l_1 and l_2), the authors were able to apply different bending moments to each beam of the specimen. In contrast to the "classic" DCB specimen, the DCB-UBM specimens rotation at the non cracked end is fixed to induce the opposing bending moment $M_1 + M_2$. The test setup used in [7] is shown in figure 4.

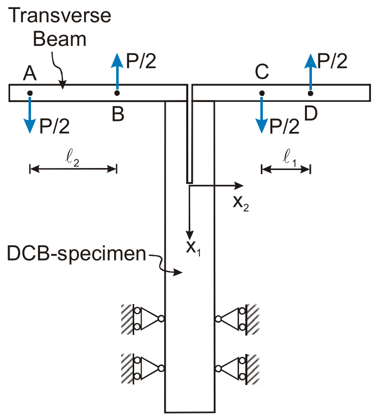

Figure 4: Apparatus used for DCB-UBM in [7].

During the test the crack opening displacement was measured in terms of the normal (δ_n) and the tangential (δ_t) opening using extensometers. Based on these measurements, the authors determined the phase angle ϕ_0 to quantify the mode mix as

$$\phi_0 = \tan^{-1} \left(\frac{\delta_t}{\delta_n} \right). \tag{12}$$

In this case a value of $\phi_0 = 0°$ reverts to pure normal opening of the crack while $\phi_0 = 90°$ is achieved by a pure tangential crack opening. The mode mixity achieved in [7] ranges from $\phi_0 = 26°$ to $\phi_0 = 75°$. As a disadvantage of the DCB-UBM the authors mention the need for a special apparatus. A clear advantage of the DCB-UBM however, is the capability of producing stable crack growth across the entire range of mode mixes. For other mixed mode tests like the MMB this is typically not the case, especially in regions of high G_{II}/G_{tot} ratios.

2.2.3 SLB test

One alternative mixed-mode test is the SLB test. The SLB test was developed by Hong and Yoon [9]. It is described as a modified ENF specimen which is subjected to a simple 3-point-bending test (see figure 5).

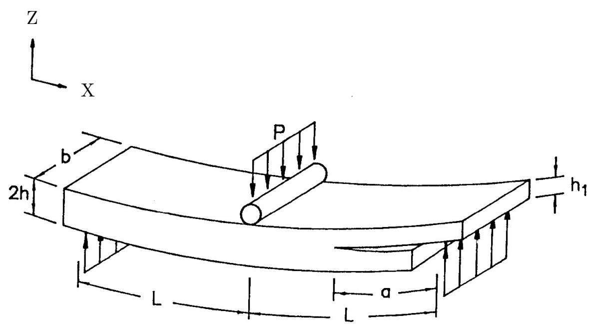

Figure 5: SLB specimen proposed by Hong and Yoon [9].

By shortening the lower of the two specimen beams it is made sure, that only the upper specimen beam experiences pure bending while the lower beam, which is only supported on the non-precracked side, can peal of, during crack propagation. This geometric modification of the specimen allows for both normal and shear opening of the crack but it has to be considered in the design of the support structure. To make sure the specimen stays level, the support carrying only the upper beam needs to be raised to compensate the thickness of the lower specimen beam. Hong and Yoon used this specimen to determine the cERR of graphite/epoxy laminates. They defined the total energy release rate G_T as the sum of the individual components in mode I and mode II

$$G_T = G_I + G_{II}. \tag{13}$$

The mixed-mode ratio in this case becomes the ratio of the mode II component to the overall energy release rate

$$\frac{G_{II}}{G_T}. \tag{14}$$

By varying the thickness of the upper beam h_1, and therefore changing its bending stiffness, while keeping the overall thickness of the specimen $2h$ constant, they were able to produce a range of mode ratios using this specimen. Over a band of thickness ratios defined as

$$\frac{h_1}{2h} \tag{15}$$

ranging from 0.3 to 0.9, they found mode ratios G_{II}/G_T from 4.7% up to 97.8%. Unlike the MMB test, the SLB test is not standardized to this day.

2.2.4 CLS test

The CLS test is another mixed-mode test alternative to the MMB test. Like the SLB test it is also not standardized, however it is frequently mentioned in literature. Brussat et al. [10] first described the test in 1977. Due to its high length to thickness ratio, the CLS specimen produces a constant G_c during crack propagation. The length of specimens described in the literature however varies quite a bit. While a 1170 mm long specimen was used in [10] other publications used much shorter specimens, for example 305 mm in [11]. The specimen described in [11] is shown in figure 6.

The specimen consists of two beams of different lengths. A precrack is introducing a fracture plane between the two beams. The lower beam extends beyond the upper beam on the precracked side. During testing the specimen is loaded in tension by clamping the non-precracked side and pulling the protruding lower beam on the opposite end. This leads to a shear loading of the crack tip (mode II). Due to the eccentric loading, the specimen is experiencing out of plane bending, introducing normal opening of the crack (mode I). Thereby a mode mixture is achieved which is highly mode II dominated.

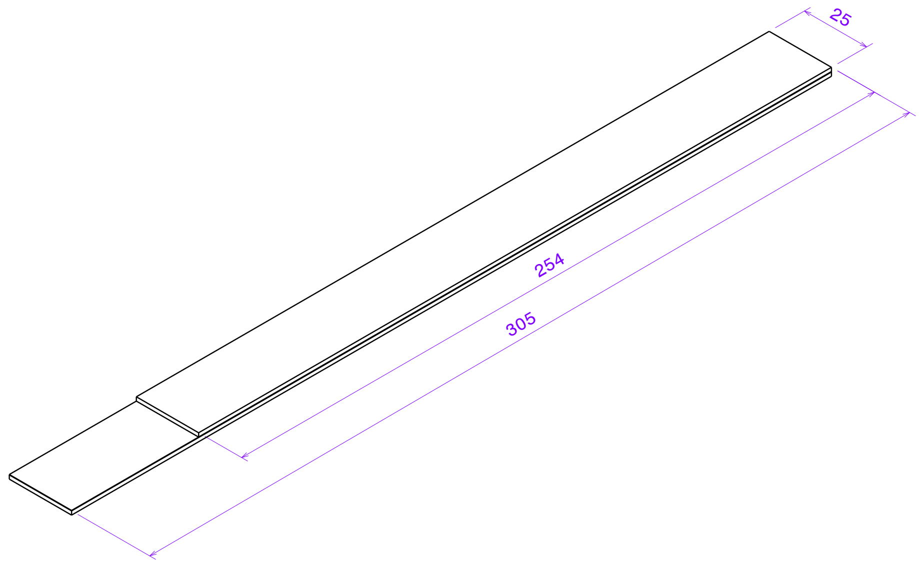

Figure 6: CLS specimen dimensioned as described in [11].

3 Crack propagation analysis

For the simulations presented in this study the commercially available fea software Abaqus was used. Abaqus offers a framework to perform crack propagation simulations using the virtual crack closure technique (VCCT). Amongst the available fracture criterions is the one by Benzeggagh and Kenane. Both the VCCT and the Benzeggagh-Kenane fracture criterion are briefly explained in the following.

3.1 Virtual crack closure technique

A method to calculate the strain energy release rates at a crack tip numerically is the VCCT. The VCCT was developed by Rybicki in 1977 [12]. Since it uses forces and displacements acting at or near the crack tip, it works well in conjunction with methods like the finite element analysis. A great overview of the VCCT was given by Krueger [13]. He explains the technique in detail and even addresses special application cases like the propagation of cracks along bi-material interfaces.

Basis for the validity of the VCCT is the idea, that the state at a crack tip does not change significantly if the crack is extended by a finite length Δa, as long as Δa is small enough. This allows the energy necessary to close the crack, to be calculated from the forces acting directly at the crack tip while using the displacements of the first row of nodes behind it. Should large deformations occur in the simulation however, local coordinate systems at the crack tip need to be introduced and the forces and displacements be transformed accordingly. A more detailed description on the topic of the local crack tip coordinate systems can be found in [13].

Since the components of the force and displacement vectors are known, the VCCT allows to calculate not only the total strain energy release rate, but its individual components G_I, G_{II} and G_{III}:

$$G_I = -\frac{1}{2\Delta A} Z_{Li}(w_{Ll} - w_{Ll*}) \tag{16}$$

$$G_{II} = -\frac{1}{2\Delta A} X_{Li}(u_{Ll} - u_{Ll*}) \tag{17}$$

$$G_{III} = -\frac{1}{2\Delta A} Y_{Li}(v_{Ll} - v_{Ll*}) \tag{18}$$

where:

$$\begin{aligned}
\Delta A &= \Delta ab \text{ (area of crack being opened)} \\
\Delta a &= \text{element edge length in direction of crack propagation} \\
\Delta b &= \text{element edge length tangential to crack front} \\
X_{Li}, Y_{Li}, Z_{Li} &= \text{force components at crack tip nodes in corresponding direction} \\
u_{Ll}, v_{Ll}, w_{Ll} &= \text{displacements of nodes behind crack tip (upper face)} \\
u_{Ll*}, v_{Ll*}, w_{Ll*} &= \text{displacements of nodes behind crack tip (lower face)}
\end{aligned}$$

The forces and displacements from equations (16) to (18) are shown in figure 7.

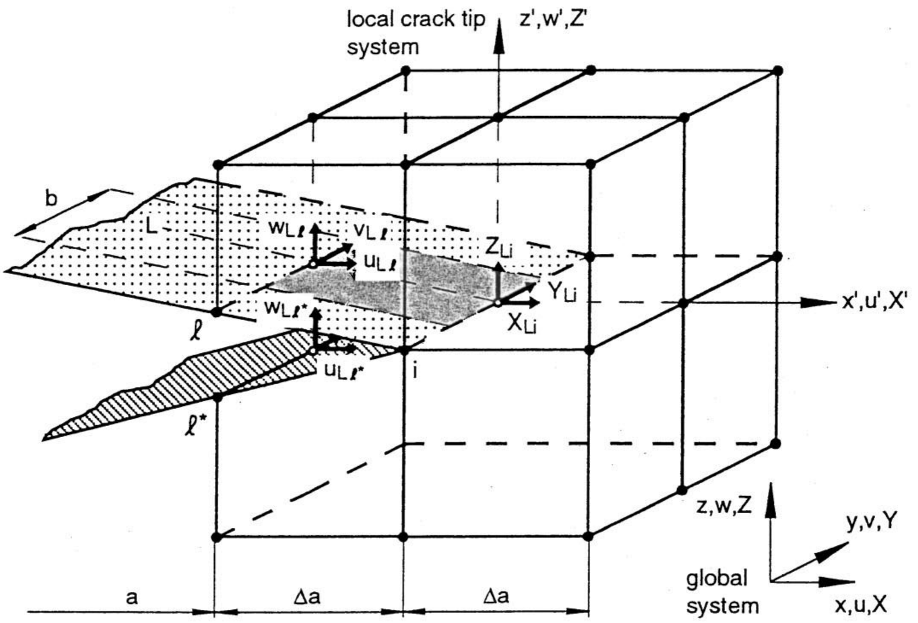

Figure 7: Nodal forces and displacements used in VCCT to calculate strain energy release rates according to [13].

3.2 Benzeggagh-Kenane fracture criterion

Benzeggagh and Kenane performed mode I, mode II and mixed-mode tests on glass-epoxy composites [14]. From these tests they determined the cERR values G_{TC} as the resistance against delamination initiation as well as the total fracture toughness G_{TR} as the resistance against crack propagation. G_{TR} was determined from recorded R-curves and is distinguishable from G_{TC} only under stable crack propagation. This means that for crack propagation under pure mode II or high G_{II}/G_T ratio, $G_{TC} \approx G_{TR}$.

To predict the onset of crack propagation, they suggested the following relation between $G_{TR,C}$ and G_{II}/G_T:

$$G_{TR,C} = G_{Ic} + (G_{IIc} - G_{Ic})\left(\frac{G_{II}}{G_T}\right)^{m_{R,C}} \tag{19}$$

The exponent $m_{R,C}$ can be determined by performing fracture mechanics tests at multiple known mode ratios G_{II}/G_T and recording the resulting $G_{TR,C}$ values. Fitting these test results to equation (19) renders $m_{R,C}$.

Benzeggagh and Kenane found, that values for $m_c = 2.6$ and $m_R = 1$ predicted the G_{TC} and G_{TR} values of the composites they tested, very successfully.

4 Simulations

The simulations presented in this work where carried out using Abaqus/Standard 2021. For crack propagation analyses using VCCT, the Abaqus VCCT framework was used. Strain energy release rates where calculated by Abaqus directly, following equations 16 through 18. Mode ratios where then calculated based on the values for G_I, G_{II} and G_{III} calculated by Abaqus. Some times mode ratios are considered as a phase angle ψ, as was presented in equations 9 and 10. Following this definition, the mode ratio ψ can take positive or negative values depending on the sign of the shear stresses in the crack interface. It was shown by [8] that fracture toughness values depend on the sign of the phase angle. The authors in [8] performed bi-axial fracture tests on end cracked specimens consisting of a glass and an epoxy layer. Their bi-axial test procedure allowed for pure tensile loading of the interface (loading direction is normal to crack plane) as well as superpositions of tensile and shear loadings. When they conducted tests with positive and negative shear loading resulting in opposing signs of ψ (-60° $< \psi <$ 90°), they found that this greatly influenced the resulting fracture toughness. Such a distinction is not made in the study presented here, since all mode ratios presented are calculated the same way Abaqus does, by using the values for G_I, G_{II} and G_{III}.

For the simulations presented in this paper a 3.25 mm thick base laminate was chosen (GFRP beams = 1.5 mm, steel layer = 0.12 mm). The layup herein is [0, 0, //, steel, 0, 0], with "//" marking the crack interface. This laminate was applied to different types of specimens to compare the resulting mode ratios. Both mode I and mode II specimens (DCB, ENF) as well as mixed-mode specimens where simulated. As discussed above, the asymmetric nature of FMLs including a precrack is especially undesirable for fracture tests aiming to produce pure mode I or mode II, since these could introduce parasitic crack opening modes. In the case of the SLB specimens the base laminate was modified to produce multiple mixed-mode ratios. An overview of the layups used in the simulations of SLB specimens is given in table 1.

Table 1: Layups used in simulations of SLB specimen ("//" = crack interface).

Specimen	Layups simulated
SLB	[0,0,steel,//,0,0], [0,steel,//,0,0,0,0], [0,0,0,steel,//,0,]

Geometric properties of all specimens are listed in tables 2. The variations in thickness of the SLB specimen due to the different layups are listed in table 3. All specimens measure 25 mm in width.

Table 2: Specimen length.

Specimen	length upper beam	length lower beam	length precrack
DCB	150 mm	150 mm	60 mm
ENF	100 mm	100 mm	35 mm
MMB	125 mm	125 mm	55 mm
CLS	254 mm	305 mm	50 mm
SLB	100 mm	65 mm	10 mm

The material properties used are based on glass fiber Seartex UD U-E-1182g/m^2-1270 mm/Epikote RIMR035c resin and 1.4310 steel. The cured single layer thickness of the UD is 0.75 mm. The thickness

Table 3: Thickness variations of the SLB specimens.

Specimen	thickness upper beam (GFRP)	thickness lower beam (GFRP)	thickness steel
SLB	0.75 mm - 4.5 mm	0.75 mm - 3.0 mm	0.12 mm

Table 4: Material properties used in simulations.

	E_x	$E_y = E_z$	ν_{xy}	ν_{xz}	ν_{yz}	G_{xy}	G_{xz}	G_{yz}
UD	42.0 GPa	12.0 GPa	0.28	0.28	0.38	2.7 GPa	2.7 GPa	4.35 GPa
Steel	180.0 GPa	165.0 GPa	0.3	0.3	0.3	69.23 GPa	69.23 GPa	63.46 GPa

values for the upper and lower beams listed in table 3 are multiples of this. The material constants used, are listed in table 4. A fiber volume fraction of $\nu_f = 50\%$ is assumed for the composite.

Fracture parameters used for the GFRP-steel interface are listed in table 5. Critical strain energy release rates G_{Ic} and G_{IIc} have been determined in previous experiments (DCB and ENF tests, unpublished). G_{IIIc} is assumed to be equal to G_{IIc}. The interaction parameter η_{BK} is unknown so far and therefore estimated. Since η_{BK} does not effect the mode ratio but only the critical strain energy release rate G_c, the findings concerning the mode ratios presented in section 4.2 are not influenced by this.

Table 5: Fracture properties used in simulations.

G_{Ic}	G_{IIc}	G_{IIIc}	η_{BK}
1.965 N/mm	3.457 N/mm	3.457 N/mm	2.0

In FMLs residual thermal stresses often result from different CTE of metal and fibrous plies. Especially when the signs of the CTE differ, as would be the case in carbon fiber-steel laminates for example, these can become significant. The signs of the CTE of GFRP and steel however are both positive. One typical hint for the presence of residual thermal stresses in FMLs is the warping after curing. However, no warping can be reported from manufacturing FMLs using the materials presented in this paper. The curing of the Epikote resin system takes place at relatively low temperatures of 80°C. Because of these observations, residual thermal stresses are assumed to be negligible in the laminates presented here and therefore are ignored in the simulations. The cooling of the laminates after curing is not simulated. When residual thermal stresses are significant however, for example from curing at elevated temperatures, these should be considered, because the observed crack opening modes will be altered by them.

4.1 Modeling of specimens

Crack interface Crack modeling using VCCT is based on a surface to surface contact interaction in Abaqus. Node pairs used in the VCCT procedure are created automatically by defining the contact interaction between two separate components and defining a VCCT crack for this interaction. This technique allows to simulate delaminations by releasing individual node pairs which are bonded initially. Such a crack was introduced in all specimens for the GFRP-steel interface meant to debond. Initial bonding was limited to a set of nodes to model the precrack. This way, nodes across the precrack interface are not bonded and the precrack can be opened. The initially bonded nodes are shown in figure 8 for the ENF specimen as an example.

Nodes on the other GFRP-steel interface where tied across the interface. The tangential behavior was modeled without friction while hard contact was chosen as normal behavior across the crack interface. Matched meshes where used between all components.

Element size The individual components of the specimens (upper and lower GFRP beam and steel layer) were meshed separately. Adjacent GFRP layers however are smeared, so that the element size in thickness direction (z-direction) is not influenced by the single layer thickness of the UD material. Specimens were partitioned so that the element size could be refined around the crack tip. The global element size in the x-direction (longitudinal) was chosen as 1 mm while global element size in y-direction

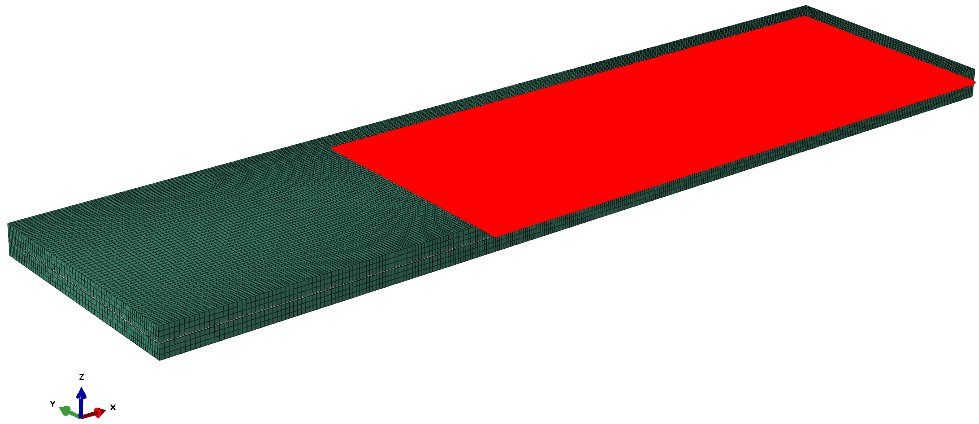

Figure 8: Set of initially bonded nodes (red) on ENF specimen. Node pairs in front of the crack tip are not tied.

(transverse) was set to 0.5 mm. In the delamination zone the element size was reduced to a constant 0.25 mm in x-direction, which is the main direction of crack propagation. At least three elements were used to mesh the individual components in the thickness direction, except for the steel layer. Due to its small thickness only one element was used in z-direction for this component.

Element type 3D solid hexader elements were used in all specimen types. Since most of the fracture mechanics tests discussed here, with the exception of the CLS test, are bending dominated problems, second order elements would be a suitable choice since these help to prevent shear locking. The VCCT framework in Abaqus however is only compatible with first order elements. Reduced integration elements (C3D8R) with hourglass control can be a good alternative here. However, Krueger and Goetze found, that C3D8I elements offer the best results when computing strain energy release rates using VCCT [15]. These types of elements feature additional internal deformation formulations to prevent shear locking and were therefore chosen for the simulatoins presented here.

Boundary conditions For all specimen types the x-axis is orientated parallel to the specimen length direction, while the y-axis follows the specimen width.

In the case of the DCB specimen, two reference points, attached to the upper and lower beam of the specimen, are introduced. These are coupled with the outer edge of the beams via coupling constraints (see figure 9). These constraints transmit all degrees of freedom (D.o.F.) except for rotations around the y-axis. All D.o.F. of the lower beams reference point are locked. The upper reference point is displaced by 50 mm in the z-direction while all other D.o.F. are also locked.

The ENF and SLB specimen are both simply supported 3-point-bending tests and use identical boundary conditions. These are applied to the outer lower edges of the specimens. All translational D.o.F. on the uncracked side are locked and only rotations around the y-axis are unconstrained. Rotations on the pre-cracked side are constrained in the same way, only translations along the x- and y-axis are free here. Loading is applied through an impactor, modeled as a rigid surface. A reference point is introduced at the center of the impactors radius. All D.o.F. of this reference point are locked, except for the translation along the z-axis, so the impactor can be displaced in this direction. Boundary conditions for the ENF specimen are shown in figure 10. Boundary conditions for the SLB specimen are analogous.

The MMB test is also a 3-point-bending test with the addition of the normal crack opening depending on the movement of the lever. In the case of the MMB specimen loading tabs were modeled to circumvent stress concentrations at the nodes where the lever attaches. Besides that, the 3-point-bend support is modeled in the same way as for the ENF or SLB specimen. The only difference is, that instead of the outer specimen edge on the precracked side, the outer edge of the loading tab is constrained. The lever was modeled as an individual, infinitely stiff component. The connection between the Yoke (load introduction) and the lever via the saddle resembles a hinge mechanism (see figure 1 in section 2.2). To model this appropriately, two reference points were introduced. The first is the load introduction point on top of the yoke (see figure 1). The second one is attached to the end of the lever. Both reference points are connected via a coupling constraint. This constraint transmits all D.o.F. except for the translation in x-direction

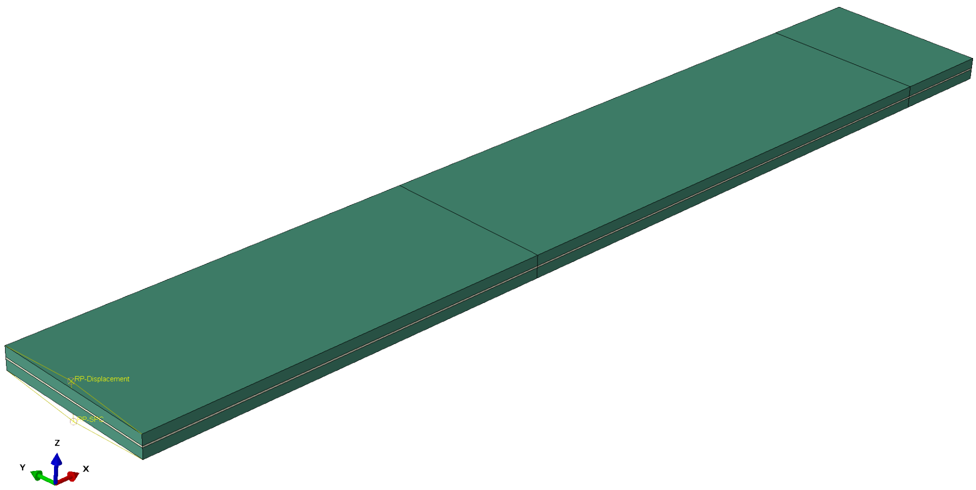

Figure 9: Coupling constraint between reference points and DCB specimen.

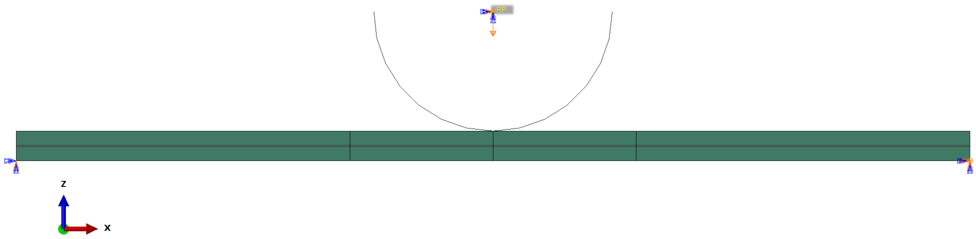

Figure 10: Boundary conditions of ENF specimen. Boundary conditions of SLB specimen are analogous.

and rotation around the y-axis. It is necessary for both reference points to move independently along the x-axis, as the yokes x- and y-coordinates remain fixed during the displacement. The x-coordinates of the lever end point change during displacement because the lever is rotating. The difference in the x-coordinates between both reference points as a result of the displacement can be seen in figure 11.

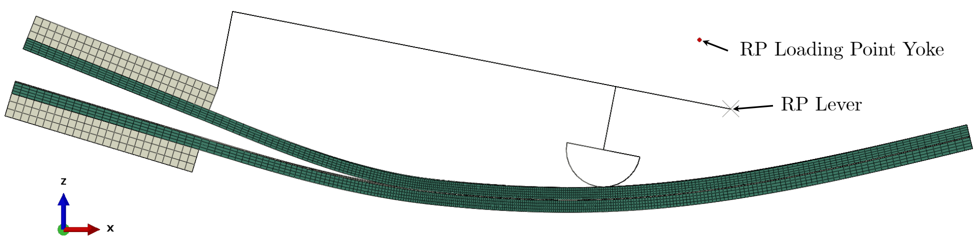

Figure 11: Boundary conditions of ENF specimen. Boundary conditions of SLB specimen are analogous.

The connection between the lever and the loading tabs of the specimen in experiments is often realized by using hinges. In the simulation, the lower edge of the lever and the top most edge of the loading tab are coincident. These coincident edges resemble the pin of the hinges used in experiments. A coupling constraint is used between these two edges to transfer loads from the lever onto the specimen. This constraint transmitts all D.o.F. except for the rotations around the y-axis (pin axis of hinge). The lever length c, which drives the mode ratio in the MMB test is the distance between the reference point of the lever and the center of the impactor pushing down onto the specimen. The boundary conditions of the MMB model are shown in figure 12.

In the CLS specimen a bending moment is introduced by the variation of thickness on the opposing ends of the specimen. This is reproduced in the simulation by using two reference points, one on each end of the specimen. Both points are located in the center of the specimen width and height. This leads

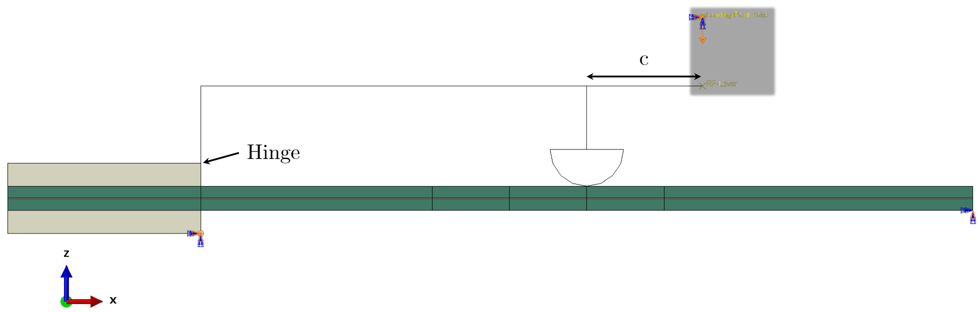

Figure 12: Boundary conditions of MMB specimen.

to different z-coordinates for both points. Each reference point is coupled with the corresponding end of the specimen (top and bottom surface). The coupling stretches across the entire specimen width and a length of 25 mm. All D.o.F. are transmitted here. This resembles the clamping of the specimen in the testing machine. On the uncracked side all D.o.F. of the reference point are locked while on the precracked side the reference point is only displaced in the x-direction by 5 mm. Boundary conditions of the SLB specimen are shown in figure 13.

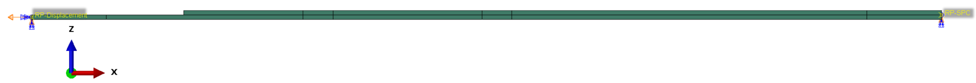

Figure 13: Boundary conditions of MMB specimen.

4.2 Results

The resulting mode ratios for the different specimen types are evaluated in this section. The range of mode ratios achieved by the proposed specimens is discussed as well as the amount of mode mix experienced by the mode I and mode II tests (DCB, ENF). The aim of these fracture tests is to achieve no mode mix of course, however, due to their asymmetric layup, this cannot be fully avoided.

Strain energy release rates are calculated directly by Abaqus. The results are evaluated at the first row of bonded nodes, forming the initially straight crack front. The presented results are taken from the moment of delamination initiation. This is the first increment in which node pairs are being released. To determine when the crack starts to propagate, the following fracture criterion is evaluated by Abaqus for every node at the crack front:

$$f = \frac{G_{equiv}}{G_{equivC}} \geqq 1.0. \tag{20}$$

G_{equiv} marks the equivalent strain energy release rate at every node, which is calculated as the sum of G_I, G_{II} and G_{III}. G_{equivC} is the critical strain energy release rate and depends on the current mode ratio. It is calculated according to the Benzeggagh-Kenane law. Unlike in equation (19), in Abaqus this is implemented as

$$G_{equivC} = G_{Ic} + (G_{IIc} - G_{Ic}) \left(\frac{G_{II} + G_{III}}{G_I + G_{II} + G_{III}} \right)^{\eta_{BK}} \tag{21}$$

so for three dimensional simulations, the contribution of G_{III} is respected.

The components of the nodal strain energy release rates where exported from Abaqus at $f \geqq 1.0$ and then used to calculate the global strain energy release rate values. This was achieved by summing up the nodal values. The global mode ratio Φ_{global} was then computed in a matter which is compatible with equation (21):

$$\Phi_{global} = \frac{G_{II,global} + G_{III,global}}{G_{I,global} + G_{II,global} + G_{III,global}}. \tag{22}$$

$G_{n,global}$ with $n \in [I, II, III]$ hereby is the sum of the nodal strain energy release value G_n across the entire crack front:

$$G_{n,global} = \sum_{1}^{nodes} G_n, n \in [I, II, III]. \tag{23}$$

Local mode ratios ϕ_{local} are calculated in the same way as global mode ratios except the nodal values G_I, G_{II} and G_{III} are used instead of the gloabl values.

The achieved mode ratios Φ_{global} and predicted $G_{equivC,global}$ values are listed in table 6. $G_{equivC,global}$ was calculated according to equation (21) using the summed up values of G_I, G_{II} and G_{III}. The data from table 6 is also plotted in figure 14. This shows the development of G_{equivC} as a function of mode-mix Φ_{global}.

Table 6: Global mode ratios Φ_{global} achieved in simulations and predicted $G_{equivC,global}$.

Specimen	Layup	length c (only MMB)	Φ_{global}	$G_{equivC,global}$
DCB	$[0, 0, //, \text{st}, 0, 0]$	-	7.94%	1.97 N/mm
ENF	$[0, 0, //, \text{st}, 0, 0]$	-	99.91%	3.45 N/mm
SLB	$[0, \text{st}, //, 0, 0, 0, 0]$	-	28.40%	2.09 N/mm
SLB	$[0, 0, \text{st}, //, 0, 0]$	-	36.40%	2.16 N/mm
SLB	$[0, 0, 0, \text{st}, //, 0]$	-	41.96%	2.23 N/mm
CLS	$[0, 0, //, \text{st}, 0, 0]$	-	65.33%	2.60 N/mm
MMB	$[0, 0, //, \text{st}, 0, 0]$	25 mm	75.61%	2.82 N/mm
MMB	$[0, 0, //, \text{st}, 0, 0]$	15 mm	99.13%	3.43 N/mm
MMB	$[0, 0, //, \text{st}, 0, 0]$	5 mm	99.86%	3.45 N/mm

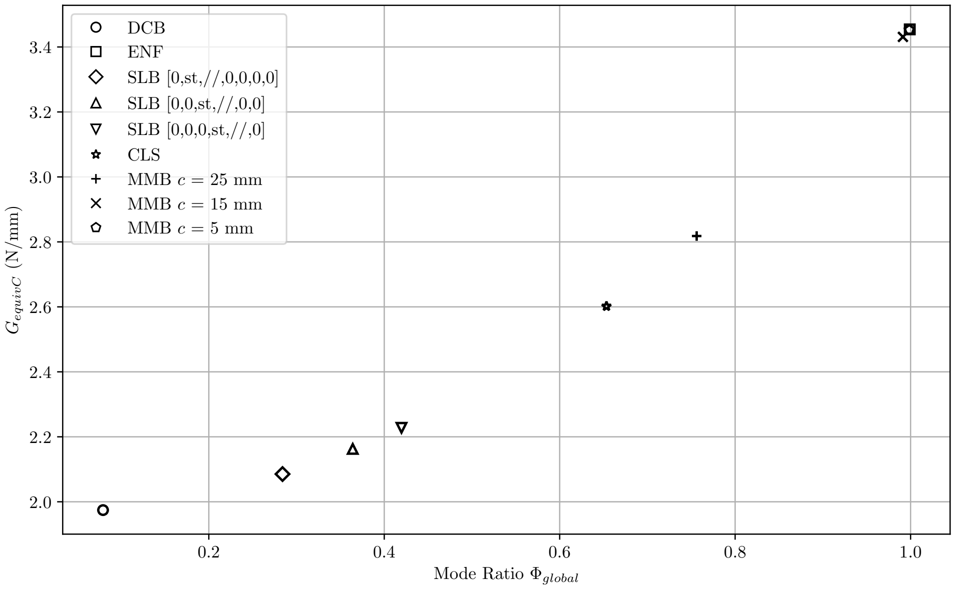

Figure 14: Predicted G_{equivC} as a function of mode-mix Φ_{global}.

The data show, that the ENF specimen produces an almost pure mode II loading condition, with a global mode mix of $\Phi_{global} = 99.9\%$. In contrast, the DCB specimen shows a significantly stronger degree of mode mixity, reaching $\Phi_{global} \approx 8\%$, despite the fact that this configuration aims to achieve $\Phi_{global} = 0\%$. The SLB specimens exhibit global mode mixities in a relatively narrow range between 28% and 42%. The CLS configuration, on the other hand, reaches a considerably higher value of $\Phi_{global} \approx$

65%. Consequently, the combined use of SLB and CLS specimens enables access to a broad spectrum of mode mixities. In the MMB simulations, the length c was systematically reduced in steps of 10 mm, from $c = 25$ mm to $c = 5$ mm. It can be observed that Φ_{global} is highly sensitive to changes of c in the high-mode-mix region. While a setting of $c = 25$ mm results in $\Phi_{global} = 75.6\%$, a reduction to $c = 15$ mm already yields $\Phi_{global} > 99\%$. This results from the effect of c on the crack opening. The displaced configurations of the MMB specimen with the three different lengths c are shown in figure 15. The figure shows the specimens at the moment where $f = 1.0$ is reached. The reduction in normal crack opening due to the change of c is clearly visible.

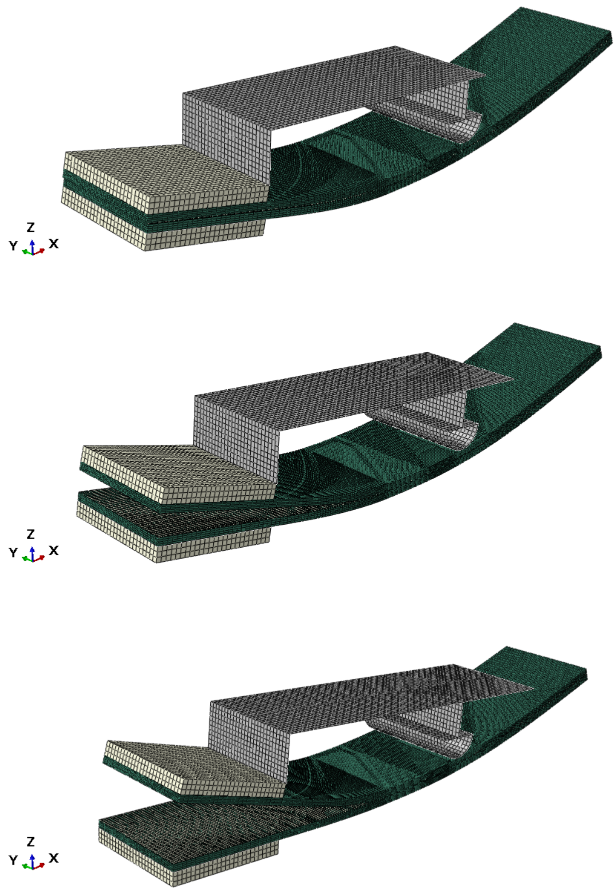

Figure 15: Displaced configuration of the MMB specimens at $f = 1.0$. $c = 5$ mm, $c = 15$ mm, $c = 25$ mm (top to bottom).

The distributions of strain energy release rates along the crack front are discussed in detail in the following. Nodal strain energy release rates are plotted over the y-coordinate of the specimens. Specimen centers are located at $y = 0$. All specimen types show symmetric distributions of strain energy release rates across the crack front. This is to be expected for the layups considered here since these feature only 0° plies and therefore are symmetric across a central plane normal to the specimen width direction.

4.2.1 DCB and ENF tests

Strain energy release rate distributions for the DCB and ENF specimens are plotted in figure 16 next to the local distribution of mode ratios.

The aim of the DCB specimen is to primarily generate G_I. G_{II} and G_{III} components are considered as parasitic contributions here. Simulation results show, that the fracture process is clearly dominated by G_I, which reaches its maximum value at the center of the specimen and decreases towards the lateral edges, where minima are observed. Mode III components are virtually non-existent along most of the crack front and only exhibit negligible values at the outermost edges. In contrast, mode II components are present across the entire specimen width, with a nearly constant distribution along the crack front.

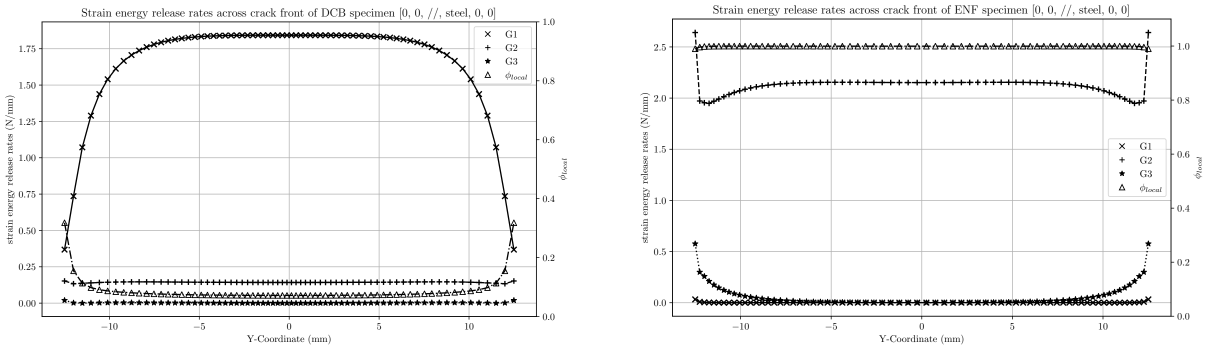

(a) DCB specimen

(b) ENF specimen

Figure 16: Strain energy release rates along crack fronts of specimens in simulated DCB and ENF tests.

Its highest values are also located at the outer edges. Due to the present of G_{II}, the DCB specimen experiences a rather high mode ratio of $\Phi_{global} = 7.94\%$.

The ENF specimen is intended to produce isolated mode II fracture behavior, so mode I and III contributions are considered parasitic here. As can be seen from the simulation results presented in figure 14, the crack opening is dominated by G_{II} with a global mode ratio of $\Phi_{global} = 99.91\%$. The maximum values of G_{II} are located near the specimen edges, while a broad plateau of nearly constant G_{II} is observed in the central region. Interestingly, G_{II} exhibits a slight decline before sharply increasing near the edges. Mode I components are effectively suppressed across the crack front, with non-zero values only at the outermost edges. This suppression is attributed to the loading mechanism of the ENF configuration, where the downward force on both beams causes the crack to be closed normal to the fracture plane and thereby preventing crack opening. G_{III} shows variation across the crack front, with values near zero at the center and increasing towards the specimen edges. The observed G_{III} results mainly from transverse contraction due to the Poisson effect. This can be seen in figure 17. Here the nodal displacements in the y-direction of the elements immediately surrounding the crack tip are plotted as vectors. The length of a vector represents the amount of displacement of the node. Displacements at the first row of nodes behind the crack tip are relevant for the calculation of G_{III} according to equation (18). The vector plot shows, that the nodes of the steel layer experience far greater displacements than their GFRP counterparts. Reducing the transverse displacement of the nodes of the steel layer behind the crack tip would therefore lower the values of G_{III}. This might be achieved by using a thicker steel layer which would experience less strain along the x-axis (longitudinal direction of the specimen). Due to the Poisson effect, this would also reduce the transverse strains in the steel layer, effectively reducing G_{III} in this region.

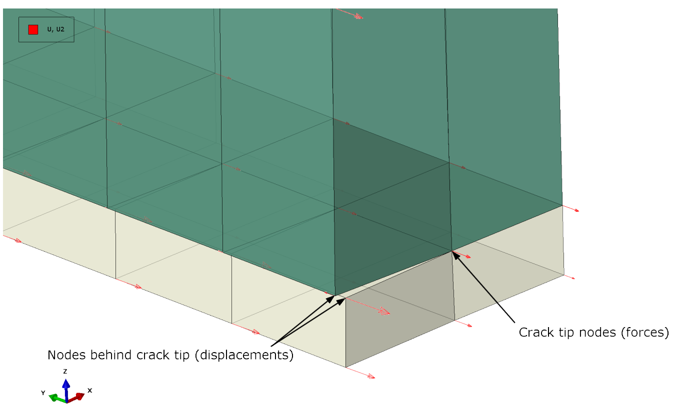

Figure 17: Nodal displacements in y-direction of elements surrounding the crack tip in ENF specimen.

4.2.2 Mixed-mode tests

Strain energy release and mode ratio distributions of the simulated SLB specimens are presented in figure 18. A comparison across various SLB layups reveals consistent characteristics in Mode III behavior. In all configurations, G_{III} is zero near the specimen center and increases towards the edges, peaking at the outermost regions. The magnitude of the mode III contribution increases with increased bending stiffness of the specimen. The distribution of G_I across the different SLB specimens shows a similar shape to that of the DCB specimen, albeit with slight variations. Specifically, in the $[0, \mathrm{st}, //, 0, 0, 0, 0]$ layup, the peak G_I values are symmetrically shifted away from the specimen center. The absolute values of G_I decrease slightly with increased thickness, and therefore bending stiffness, of the upper specimen beam. More substantial variations are observed in the distribution of G_{II}. As bending stiffness increases, the variation of G_{II} along the crack front becomes more pronounced. The difference between the edge and center values increases, and so does the absolute magnitude of G_{II}. Consequently, the ratio G_I/G_{II} decreases, primarily due to the increasing mode II contribution.

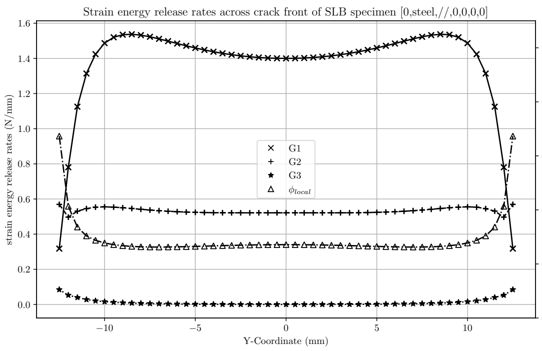

(a) SLB [0,steel,//,0,0,0,0]

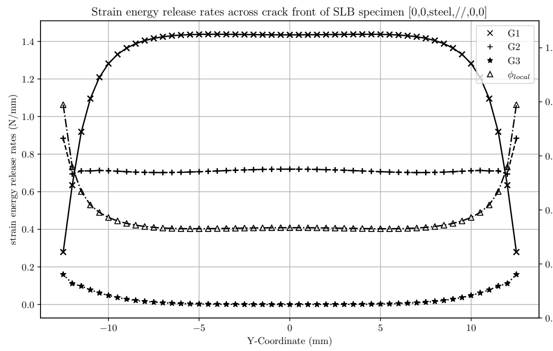

(b) SLB [0,0,steel,//,0,0]

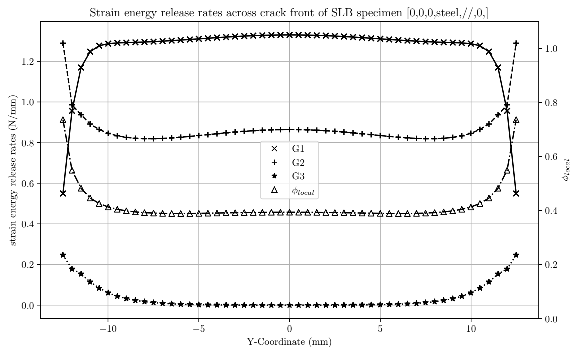

(c) SLB [0,0,0,steel,//,0]

Figure 18: Strain energy release rates along crack fronts of simulated SLB tests.

Strain energy release rate and mode ratio distributions of the simulated CLS specimen are presented in figure 19. The CLS specimen is predominantly governed by mode II loading. The G_{II} distribution forms a plateau in the central region, gradually decreasing toward the specimen edges. Compared to the ENF specimen, this drop-off is more extended along the width of the crack front. Maximum G_{II} values are again found at the edges of the specimen. The G_I distribution resembles that of the DCB specimen, with a central plateau and decreasing values toward the edges. Across the entire crack front, the mode II contribution exceeds that of mode I. The G_{III} distribution observed in the CLS specimen is comparable to those in the ENF and SLB configurations, meaning G_{III} is essentially zero in the center with increasing values toward the outer edges.

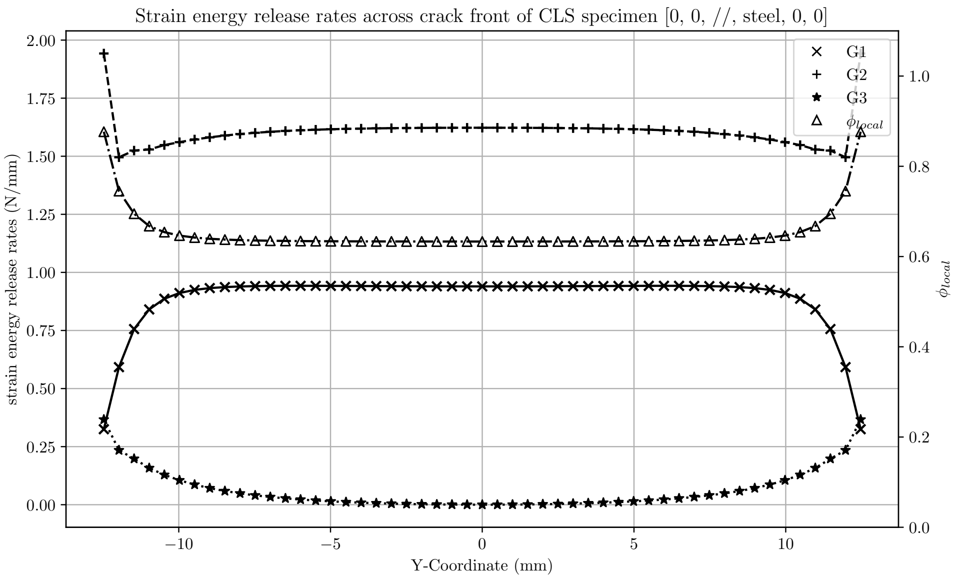

Figure 19: Strain energy release rate distributions along the crack front of CLS specimen from simulations.

Distributions of strain energy release rate and mode ratio distribution for simulated MMB specimens with three different lever lengths c are shown in figure 20. For the MMB specimen with a length c = 25 mm, mode II dominates the energy release rate distribution. Uniquely, the minimum value of G_{II} is found at the specimen center, in contrast to the other mode II-dominated configurations. Nevertheless, consistent with previous observations, G_{II} reaches peak values near the edges. The distribution of G_I closely resembles that observed in the SLB $[0, \mathrm{st}, //, 0, 0, 0, 0]$ configuration, with maxima symmetrically shifted away from the center. Mode III components remain negligible across the crack front except at the specimen edges where these exceed even G_I. A further increase in the contribution of mode II is observed when c is reduced to 15 mm and 5 mm. Mode I becomes effectively negligible throughout the entire crack front. In contrast, G_{III} remains zero in the center but rises toward the edges, becoming more significant than G_I in these configurations.

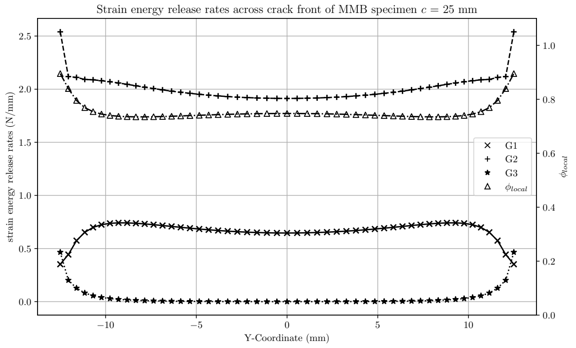

(a) MMB $c = 25$ mm

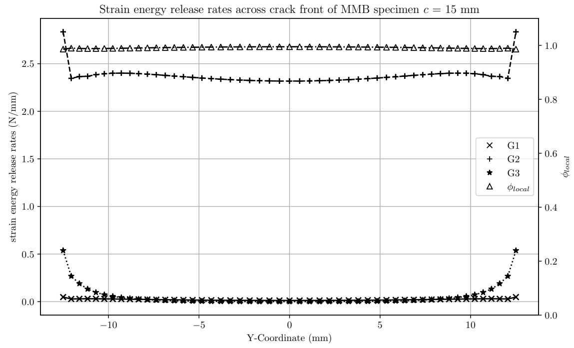

(b) MMB $c = 15$ mm

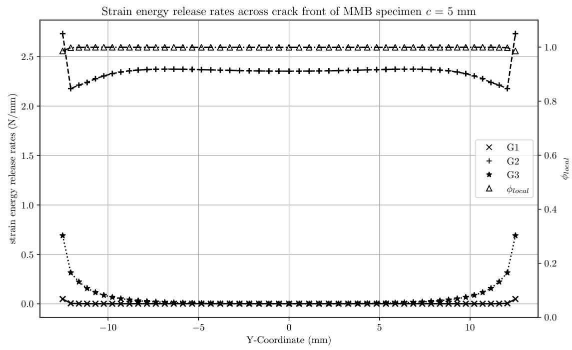

(c) MMB $c = 5$ mm

Figure 20: Strain energy release rates along crack fronts of simulated MMB specimens with varied lever length c.

4.3 Discussion

The degree of mode mix differs significantly between DCB and ENF specimens. While the DCB specimen exhibits a notable influence of Mode II contributions ($\phi \approx 8\%$), the effect in the ENF specimen is nearly negligible ($\phi \approx 99\%$). In the case of DCB, the presence of mode II crack opening modes increases the critical strain energy release rate G_c, leading to the risk of overestimating of G_{Ic}, when testing the layup presented here. To mitigate this effect, the layup of the DCB specimen should be reconsidered in order to reduce the G_{II} contribution. Two alternatives present themselves:

One potential solution includes increasing the number of glass plies while minimizing the thickness of the steel layer. This approach would reduce the effective asymmetry of the specimen by decreasing the relative distance between the fracture plane and the mid-plane, thereby approximating a more symmetric specimen geometry.

Alternatively one could try to compensate the increased bending stiffness of the beam containing the steel layer by introducing additional glass layers into the monolithic beam. For example, a layup of [0,0,//,steel,0,0] could be modified to [0,0,0,//,steel,0,0]. However, since only fixed increments in thickness can be used here, it might be impossible to find a layup with a small enough mode ratio ϕ this way.

The proposed SLB specimen provides only a narrow window of mode ratios ($28\% < \phi < 42\%$). To capture critical strain energy release rates at higher mode ratios, it would be beneficial to accompany SLB testing with CLS testing, as the CLS specimen presented here produces substantially higher mode ratios ($\phi \approx 65\%$). However, from a practical standpoint, it would be ideal to rely on a single specimen type across the entire range of mode ratios, thereby minimizing manufacturing and testing efforts. Consequently, the SLB specimen would need further modifications to achieve higher values of ϕ. Potential modifications include:

Altering the thickness ratio: This could be achieved by adding more glass layers to the upper beam, thereby increasing asymmetry. For instance, a layup such as [0,0,0,steel,//,0] may be changed to [0,0,0,0,0,steel,//,0], effectively increasing the thickness ratio as defined by Hong and Yoon from $h_1/2h = 0.76$ to $h_1/2h = 0.84$.

Changing the crack interface position: Shifting the steel layer into the lower beam, e.g., from [0, 0, steel, //, 0, 0] to [0, 0, //, steel, 0, 0], however, both approaches introduce distinct risks. Increasing asymmetry in the layup raises the likelyhood of warping during curing at elevated temperatures. Meanwhile, relocating the crack interface complicates specimen manufacturing, as the required step in the SLB specimen becomes more difficult to produce by milling. In this case, the steel layer must be cut while not being fixed to the underlying GFRP layers due to the presence of the pre-crack.

All modifications to specimens mentioned above would still have to be simulated first, so their effectiveness can be quantified.

5 Conclusion

The ENF specimen demonstrated superior resistance against parasitic mode I contributions due to the nature of the three-point bending configuration, which inherently prevents the normal opening of the crack interface.

In contrast, the DCB specimen exhibited stronger influence from parasitic mode II crack openings. This parasitic effect may lead to an overestimation of cERR in mode I, as an increase in G_{II} at the crack tip can artificially elevate the apparent fracture toughness. Further investigation is required to develop a DCB configuration specifically optimized for FMLs that ensures a more isolated G_I contribution.

Various mixed-mode ratios Φ could be achieved using the SLB specimen configuration. Consequently, this specimen type is well suited for the determination of fracture toughness values of FMLs under mode I-dominated conditions. To obtain crack-driving force distributions dominated by mode II G_{II}, further modification of the SLB configuration would be required.

However, depending on the specific manufacturing processes employed, the production of increasingly thick laminates for such specimen designs may become impractical. In such cases, alternative specimen types that inherently promote higher G_{II} contributions, such as the CLS configuration, may present a more feasible solution. Using the CLS specimen, global mode mixities Φ_{global} in the desired mode II-dominated range could be successfully achieved. Moreover, through variations in beam thicknesses the mode II contribution may potentially be increased even further.

Nonetheless, the highest mode II energy release rates were still only attainable using the MMB configuration with c set to specifically short lengths (c < 25 mm). This configuration remains the most effective for achieving strongly mode II-dominated fracture conditions in FMLs. Where mode ratios below Φ = 65% are sufficient, SLB and CLS specimens present a practical alternative for evaluating critical strain energy release rates, offering reduced experimental effort compared to the more intricate MMB configuration.

Acknowledgements

The work presented in this paper was funded by the Federal Ministry for Economic Affairs and Climate Action of the Federal Republic of Germany under the project "HoBi - High strength bolted connections for rotor blades of wind turbines" (Grant No. 03EE3083A).

References

[1] Beyland L, Hindersmann A, Bäns C, Mahrholz T and Kaps R 2021 Hybrid Materials and Conical Bolts for High-Strength Bolted Joints *Wind Turbine Blade Manufacture* URL `https://elib.dlr.de/145845/`

[2] Petersen E 2019 *Auslegung des Metalllagenauslaufs bei lokaler Stahlhybridisierung von Kohlenstofffaser-Kunststoff-Laminaten* phdthesis Technischen Universität Carolo-Wilhelmina zu Braunschweig

[3] ASTM International 2013 Standard Test Method for Mode I Interlaminar Fracture Toughness of Unidirectional Fiber-Reinforced Polymer Matrix Composites DOI:10.1520/D5528-01

[4] ASTM International 2019 Standard Test Method for Determination of the Mode II Interlaminar Fracture Toughness of Unidirectional Fiber-Reinforced Polymer Matrix Composites DOI:10.1520/D7905_D7905M-19E01

[5] ASTM International 2006 Standard Test Method for Mixed Mode I-Mode II Interlaminar Fracture Toughness of Unidirectional Fiber Reinforced Polymer Matrix Composites DOI:10.1520/D6671_D6671M-06

[6] Fernández M V, de Moura M F S F, da Silva L F M and Marques A T 2013 *Composites Part A: Applied Science and Manufacturing* **44** 63–69 ISSN 1359-835X URL https://www.sciencedirect.com/science/article/pii/S1359835X12002497

[7] Sørensen B, Jørgensen K, Jacobsen T K and Østergaard R C 2004 *A general mixed mode fracture mechanics test specimen: The DCB-specimen loaded with uneven bending moments* (*Denmark. Forskningscenter Risoe. Risoe-R* no 1394(EN)) (Risø National Laboratory) ISBN 87-550-3186-2

[8] Liechti K and Chai Y S 1992 *Journal of Applied Mechanics* **59**

[9] Yoon S H and Hong C S 1990 *International Journal of Fracture* **43** R3–R9 ISSN 1573-2673

[10] Brussat T R, Chiu S T and Mostovoy S 1977 Fracture mechanicsfor structural adhesive bonds resreport Burbank, CA

[11] Johnson W S 1986 Stress analysis of the cracked lap shear specimens: An ASTM round robin resreport 89006 National Aeronautics and Space Administration Langley Research Center, Hampton, VA URL https://ntrs.nasa.gov/citations/19860021599

[12] Rybicki E F and Kanninen M F 1977 *Engineering Fracture Mechanics* **9** 931–938 ISSN 0013-7944 URL https://www.sciencedirect.com/science/article/pii/0013794477900133

[13] Krueger R 2004 *Applied Mechanics Reviews* **57** 109–143 ISSN 0003-6900 URL https://doi.org/10.1115/1.1595677

[14] Benzeggagh M L and Kenane M 1996 *Composites Science and Technology* **56** 439–449 ISSN 0266-3538 URL https://www.sciencedirect.com/science/article/pii/026635389600005X

[15] Krueger R, Goetze D and Ransom J F 2013 Influence of Finite Element Software on Energy Release Rates Computed Using the Virtual Crack Closure Technique URL https://api.semanticscholar.org/CorpusID:137044374